Electronic supporting information (ESI)

Molecular and thin film properties of cobalt half-sandwich compounds for optoelectronic application

Maxwell Reinhardt,[‡a] Simon Dalgleish,*[‡bc] Yoshiaki Shuku,[c] Louisa Reissig,[c] Michio M. Matsushita,[c] Jason Crain,[d] Kunio Awaga[c] and Neil Robertson*[a]

a) EaStCHEM School of Chemistry, University of Edinburgh, West Mains Road, Edinburgh EH9 3JJ, UK. E-mail: neil.robertson@ed.ac.uk.

b) Institute for Advanced Research, Nagoya University, Furo-cho, Chikusa-ku, 464-8601, Nagoya, Japan. E-mail: s.dalgleish@nagoya-u.jp,

c) Department of Chemistry and Research Center for Materials Science, Nagoya University, Furo-cho, Chikusa-ku, 464-8602 Nagoya, Japan.

d) School of Physics and Astronomy, University of Edinburgh, James Clerk Maxwell Building, Peter Guthrie Tait Road, Edinburgh EH9 3FD, UK.

Contents:

Tables:

Figures:

Synthetic Procedures

($\eta^5$$C_5H_5$)Co(CO)$I_2$. The synthesis was derived from the method of King.[1] Dicarbonylcyclopentadienylcobalt(I), $CpCo(CO)_2$ (1.0 g, 5.67 mmol), was dissolved in MeOH (20 ml) under N_2. Iodine (1.41 g, 5.67 mmol) was added to the stirred solution over 20 min, resulting in the evolution of CO, and formation of a black precipitate. The mixture was concentrated to half volume on a rotary evaporator before filtering under vacuum. The black residue was extracted into DCM (100 ml) and evaporated to dryness to give a black, microcrystalline product (1.915 g, 83%). Calc. for $C_6H_5CoI_2O$: C, 17.76; H, 1.24; N, 0.00. Found: C, 17.79; H, 1.14; N, 0.00. ^{1}H-NMR (500 MHz, $CDCl_3$): δ 5.69 (5H, s). ^{13}C-NMR (500 MHz, $CDCl_3$): δ 89.42 (5 × *C*H). MS (+ESI): *m*/*z* 437.31 ([M+CH_3OH]$^+$, 100%). IR (KBr, cm^{-1}) *ν* 2924 (w), 2360 (s), 2335 (s), 2063 (s), 1869 (w), 1844 (w), 1791 (w), 1772 (w), 1734 (m), 1716 (m), 1699 (m), 1684 (m), 1670 (w), 1653 (s), 1635 (m), 1616 (w), 1576 (w), 1558 (s), 1541 (s), 1522 (m), 1506 (s), 1489 (w), 1473 (w), 1456 (m), 1437 (w), 1419 (m), 1396 (w), 1070 (m), 1043 (m), 837 (s), 667 (m), 600 (m).

($\eta^5$$C_5H_5$)Co($(NH)_2C_6H_4$) – CpCo(DAbnz). The synthesis was derived from the method of Heck.[2] $CpCo(CO)I_2$ (0.812 g, 2 mmol) and 1,2-diaminobenzene (0.216 g, 2 mmol) were dissolved in dry DCM (10 ml) and stirred at RT for 3 h. The resultant black solid was filtered and dried. The crude intermediate was re-suspended in diethyl ether (Et_2O, 25 ml) and added to a separating funnel with a solution of NaOH (2 g, 50 mmol) in H_2O (20 ml). The layers were shaken vigorously, resulting in the organic layer turning very dark red in colour. The aqueous phase was removed, and the organic phase washed twice with water (2 × 25 ml). The diethyl ether solution was evaporated to dryness on a rotary evaporator, producing a black crystalline solid with a green hue (0.373 g, 81%). Calc. for $C_{11}H_{11}CoN_2$: C, 57.40; H, 4.82; N, 12.17. Found: C, 57.50; H, 4.76; N, 12.10. ^{1}H-NMR (500 MHz, $CDCl_3$): δ 5.02 (5H, s), 6.96 (4H, m), 9.57 (2H, s). ^{13}C-NMR (500 MHz, $CDCl_3$): δ 75.61 (5 × *C*H), 116.97 (2 × *C*H), 120.15 (2 × *C*H), 151.83 (2 × *C*q). MS (+ESI): *m*/*z* 231.13 ([M+H]$^+$, 100%), 196.79 ([Co(DAbnz)+CH_3OH]$^+$, 25%), 182.78 ([Co(DAbnz)+H_2O]$^+$, 24%). IR (KBr, cm^{-1}) *ν* 3466 (s, br), 3432 (s, br), 1638 (s), 1472 (w), 1412 (w), 1372 (m), 1340 (w), 1302 (w), 1198 (w), 1108 (m), 1048 (w), 1000 (m), 914 (w), 816 (m), 744 (s), 670 (w), 656 (w), 574 (w).

NMR Data

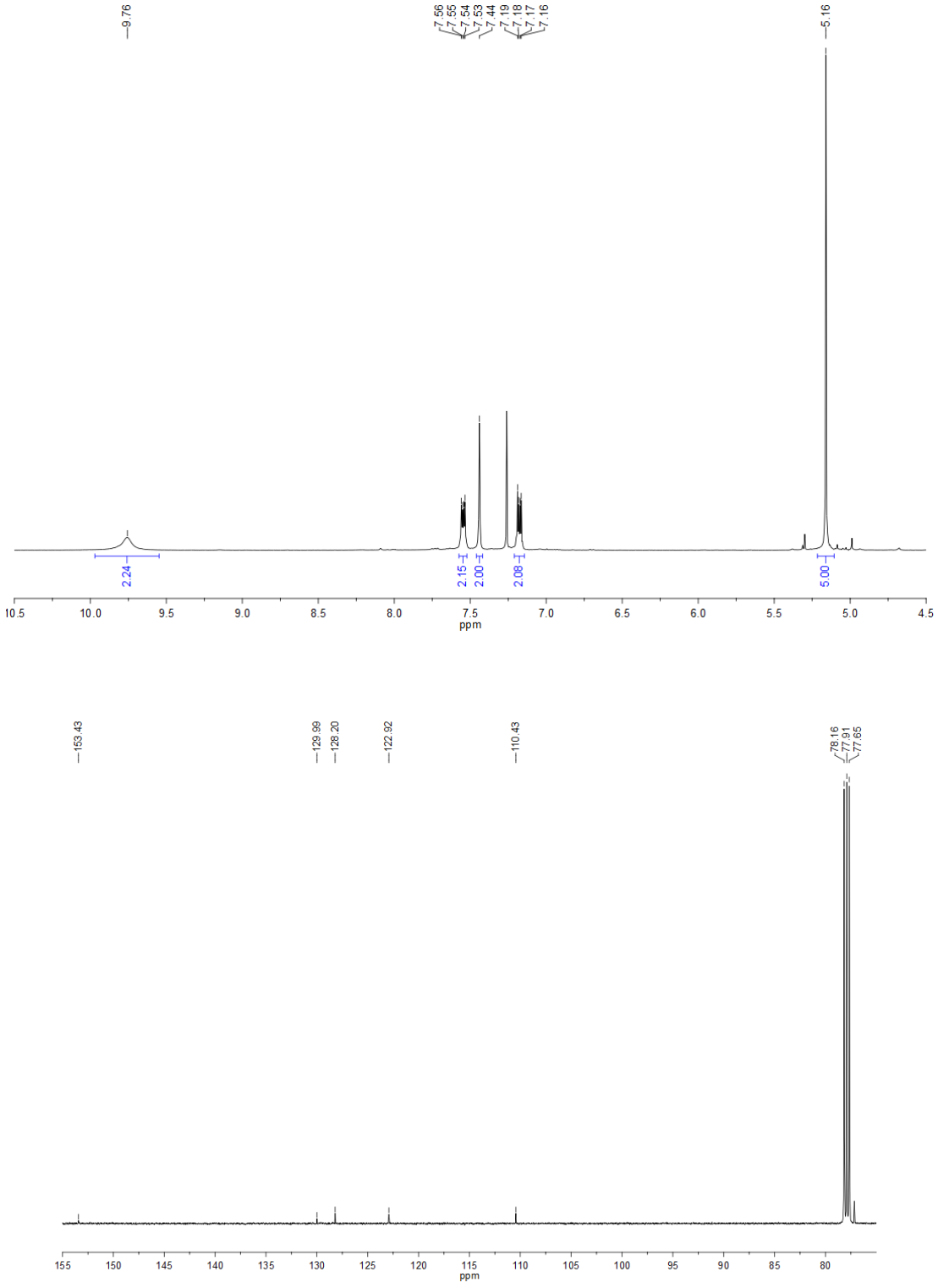

***Figure S1**: ^{1}H NMR (upper) and ^{13}C-NMR (lower) spectra of CpCo(DAnap) in $CDCl_3$.*

Structural Data

Table S1: *Crystallographic data and structure refinement details for CpCo(DAnap).*

	CpCo(DAnap)
Chemical formula	$C_{15}H_{13}CoN_2$
Crystal size / mm^3	0.11 × 0.05 × 0.03
Crystal colour, shape	Green block
Fw	280.21
Crystal system	Orthorhombic
Space group	*P*bca
a, *b*, *c* / Å	8.0533(8), 25.607(3), 45.045(5)
α, β, γ / °	90.0
V / $Å^3$	9289.3(16)
Z	32
Calc. density / g cm^{-3}	1.603
μ / mm^{-1}	14.578
T / K	123
Radiation, λ / Å	Mo-Kα, 0.71075
θ range / °	3.11 to 27.49
Index ranges	h -9 to 10
	k -33 to 33
	l -44 to 58
Refinement method	Full-matrix least-squares on F^2
Absorption correction	Multi-scan
T_{min}, T_{max}	0.685, 0.957
Structure solution	Direct methods (Sir97)
R_{int}	0.054
Collected, independent, observed [$I > 2\sigma(I)$]	48629, 10445, 8255
Reflections used	10445
Parameters / restraints	649 / 0
R [$I > 2\sigma(I)$], R_w [all], GOF	0.0510, 0.1138, 1.089
$\Delta\rho_{max}$, $\Delta\rho_{min}$ (e $Å^{-3}$)	0.78, -0.50

$^a R = \Sigma||F_o| - |F_c||/\Sigma|F_o|$. $^b R_w = [\Sigma w(|F_o| - |F_c|)^2/\Sigma w|F_o|^2]^{1/2}$.

Table S2: *Unit cell parameters and reliability factors obtained from Rietveld refinement of powder data of CpCo(DAbnz) and CpCo(DAnap).*[3]

	CpCo(DAbnz) Powder	CpCo(DAbnz) SC*	CpCo(DAnap) Powder	CpCo(DAnap) SC
Space group	P21/n	P21/n	Pbca	Pbca
a / Å	17.8129(9)	17.817(5)	8.1071(5)	8.0533(8)
b / Å	8.8612(9)	8.865(2)	25.5678(5)	25.607(3)
c / Å	12.4825(3)	12.479(3)	45.4773(6)	45.045(5)
α / °	90	90	90	90.0
β / °	94.6973(4)	94.70(2)	90	90.0
γ / °	90	90	89.4290(4)	90.0
V / Å3	1963.750(5)	1964.4(6)	9426.112(4)	9289.3(16)
Z	8	8	32	32
λ (Å)	1.5418	1.5418	1.5418	1.5418
2θ range (°)	2-30	3-45	6-30	3-27.5
Rp (%)	5.67		13.98	
Rwp (%)	8.17		26.18	
Rexp (%)	5.13		2.95	
χ2 (GoF)	1.592		8.885	

*From Rheingold.[4]

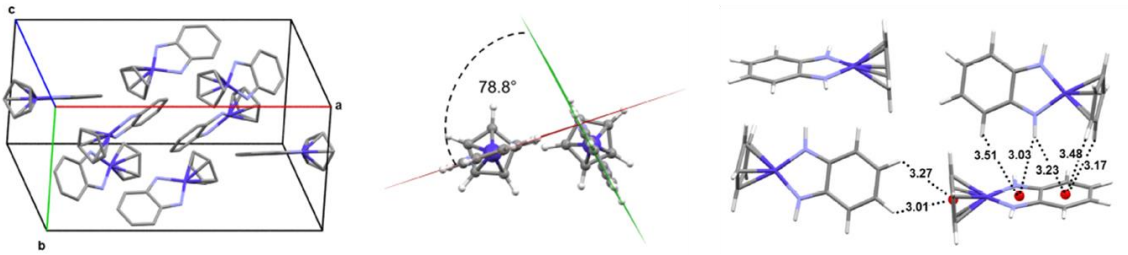

Figure S2*: Unit cell (left) and angles between adjacent molecular LS planes in the asymmetric unit (middle) and intermolecular short contacts (right) for CpCo(DAbnz). H-atoms are omitted from the unit cell diagram for clarity.*

Electrochemical Data

Table S3: *Selected electrochemical values observed from CV for CpCo(DAbnz) and CpCo(DAnap) in MeCN with 0.3 M TBABF$_4$ supporting electrolyte.*

Complex	$E_{1/2}^{\mathrm{red}}$ (V)	ΔE (mV)	$\lvert i_{pa}/i_{pc} \rvert$	$E_{1/2}^{\mathrm{ox}}$ (V)	ΔE (mV)	$\lvert i_{pa}/i_{pc} \rvert$	$E_{\mathrm{gap}}^{\mathrm{CV}}$ (eV)
CpCo(DAbnz)	-1.83[B]	90	0.61	-0.13[A]	70	1.13	1.55
CpCo(DAnap)	-1.52[A]	100	1.04	-0.10[C]	*n/a*	*n/a*	1.26

[†]Scan rate = 0.1 V s^{-1}. Potentials are referenced *vs*. Fc/Fc^{+}. For processes defined as irreversible, $E_{1/2}^{\mathrm{red/ox}}$ = (E_{p} + $E_{\mathrm{p/2}}$)/2 and $\Delta E_{\mathrm{p/2}}$ = (E_{p} − $E_{\mathrm{p/2}}$), where $E_{\mathrm{p/2}}$ is the half-peak potential. $E_{\mathrm{gap}}^{\mathrm{CV}}$ is determined from the onset of the waves. [A]Electrochemically-reversible redox process. [B]Partially-reversible redox process (presence of redox activity within 200 mV of the peak potential). [C]Electrochemically-irreversible redox process.

Table S4: *Selected electrochemical values observed from DPV for CpCo(DAbnz) and CpCo(DAnap) in MeCN with 0.3 M TBABF$_4$ supporting electrolyte.*

Complex	$E_{1/2}^{\mathrm{red}}$ (V)	ΔE (mV)	$\lvert i_{pa}/i_{pc} \rvert$	$E_{1/2}^{\mathrm{ox}}$ (V)	ΔE (mV)	$\lvert i_{pa}/i_{pc} \rvert$	$E_{\mathrm{gap}}^{\mathrm{DPV}}$ (eV)
CpCo(DAbnz)	-1.84[B]	99	1.44	-0.12[A]	33	0.64	1.45
CpCo(DAnap)	-1.57[B]	*n/a*	*n/a*	-0.13[C]	235	22.7	1.20

[†]Scan rate = 0.1 V s^{-1}. Potentials are referenced *vs*. Fc/Fc^{+}. For processes defined as irreversible, $E_{1/2}^{\mathrm{red/ox}}$ = E_{p}. [A]Electrochemically-reversible redox process. [B]Partially-reversible redox process. [C]Electrochemically-irreversible redox process.

Spectroscopic Data

Table S5: *Peak absorption maxima from electronic spectra in MeCN solution.*[*]

Complex	λ^{abs}_{max}	$\lambda^{abs,film}_{max}$	λ^{refl}_{max}
CpCo(DAbnz)	740 [650]	*n/a*	788
	523 [24,500]		536
	290 [7,000]		
	249 [11,500]		
CpCo(DAnap)	940 [560]	1060 [2,110]	1082
	560 [29,820]	490 [4,250]	576
	278 [49,800]	266 [16,580]	
	241 [36,100]		

[*]Peak absorption maxima positions are measured in nm. Square brackets represent the molar extinction coefficient (mol^{-1} dm^3 cm^{-1}).

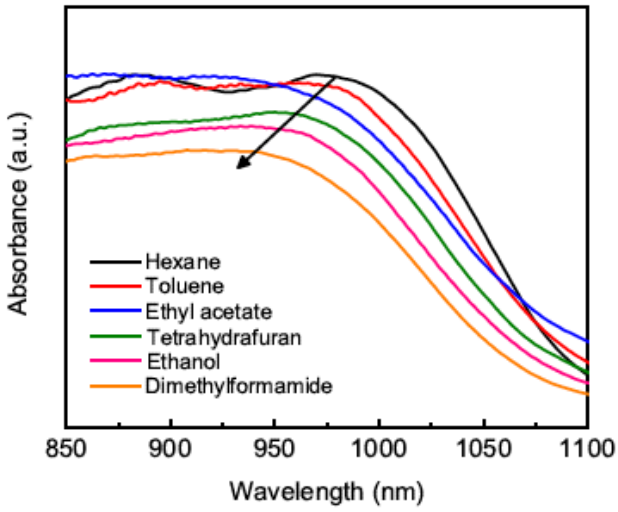

Figure S3: *Solvatochromic shift of the NIR peak of CpCo(DAnap) showing a hypsochromic shift from a peak maximum position of 975 nm in hexane to 903 in DMF. There is a second peak observable on the blue edge of the peak (ca. 880 nm) in low polarity solvents (hexane, toluene and ethyl acetate).*

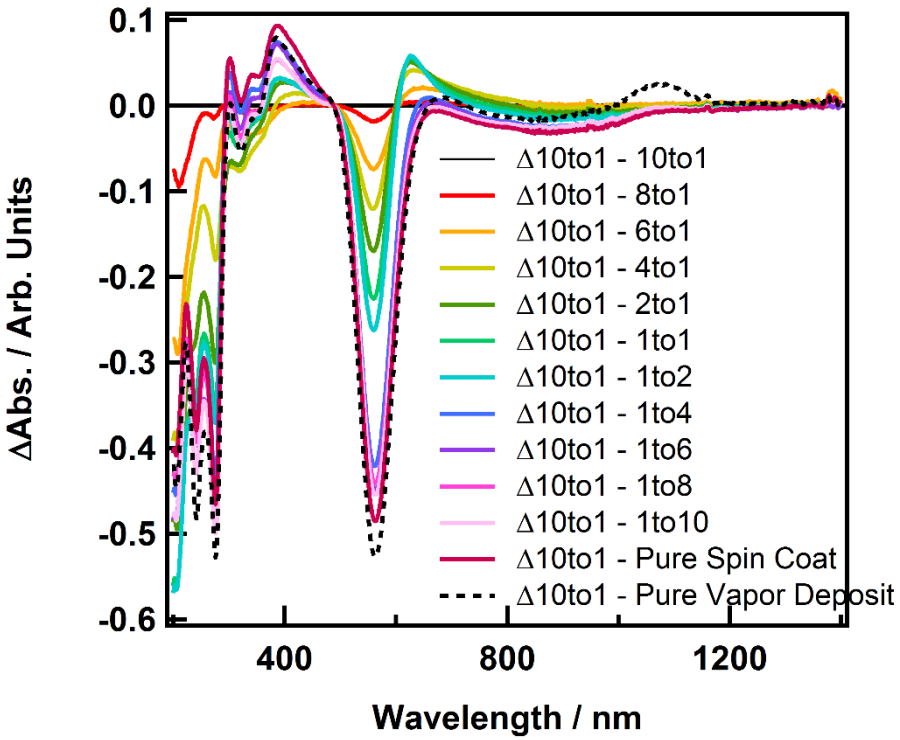

Figure S4: *Difference spectra of thin films of CpCo(DAnap) dispersed at different loadings in a PMMA matrix, normalized to common intercept in solution and thin-film data, as in Figure 3b.*

Computational Data

Table S6: *Selected geometry parameters and orbital energies calculated from various levels of theory*[*] *for CpCo(DAbnz).*[**]

Functional	Co ECP/basis set	Co···Cp (Å)	E_{HOMO} (eV)	E_{LUMO} (eV)	*E*gap (eV)
B3LYP	LAND2DZ	1.724	-5.05	-2.25	2.80
BP86	LAND2DZ	1.672	-4.39	-2.94	1.45
TPSS	LAND2DZ	1.655	-4.30	-2.75	1.55

[*]The basis set 6-31G(d,p) was used for the ligand atoms. All calculations were performed using the PCM to model solvent interactions with MeCN as the solvent. [**]Crystal structure: Co···Cp = 1.649 Å. Electrochemical values: E^{CV}_{HOMO} = -4.42 eV, E^{opt}_{LUMO} = -2.99 eV, E^{opt}_{gap} = 1.43 eV.

Table S7: *Selected geometry parameters and orbital energies calculated from various levels of theory*[*] *for CpCo(DAnap).*[**]

Functional	Co ECP/basis set	Co···Cp (Å)	E_{HOMO} (eV)	E_{LUMO} (eV)	*E*gap (eV)
B3LYP	LAND2DZ	1.720	-4.95	-2.55	2.41
BP86	LAND2DZ	1.670	-4.26	-3.22	1.05
	SDD/MHF10	1.672	-4.25	-3.20	1.05
TPSS	LAND2DZ	1.654	-4.33	-3.21	1.12
	6-311G(d,p)	1.601	-4.02	-2.78	1.28
	SDD/MHF10	1.659	-4.14	-3.01	1.12

[*]The basis set 6-31G(d,p) was used for the ligand atoms. All calculations were performed using the PCM to model solvent interactions with MeCN as the solvent. [**]Crystal structure: Co···Cp = 1.656-1.663 Å. Electrochemical values: E^{CV}_{HOMO} = -4.46 eV, E^{opt}_{LUMO} = -3.31 eV, E^{opt}_{gap} = 1.15 eV.

Table S8: *Calculated and experimental peak maximum excitation energies (in nm) and assignments of frontier orbital transitions from TD-DFT calculations.*[*]

Complex	Calc. peak max.	Exp. peak max.	Majority orbital contributions	
CpCo(DAbnz)	754 [0.0034]	740 [650]	HOMO → LUMO (94%)	
	471 [0.4262]	523 [24500]	H-1 → LUMO (97%)	
	273 [0.3019]	290 [7000]	HOMO → L+3 (46%)	H-6 → LUMO (16%)
	252 [0.0969]	249 [11500]	H-8 → LUMO (56%)	H-4 → L+3 (13%)
CpCo(DAnap)	949 [0.0076]	940 [560]	HOMO → LUMO (98%)	
	501 [0.6031]	560 [29820]	H-2 → LUMO (50%)	H-1 → LUMO (47%)
	296 [0.5531]	278 [49800]	HOMO → L+3 (37%)	H-3 → L+3 (24%)
	271 [0.0404]	241 [36100]	HOMO → L+7 (70%)	

[*]BP86 functional with 6-31G(d,p) basis set used for ligand atoms and LANL2DZ ECP used for Co. Calculated oscillator strengths and molar absorptivities are represented in square brackets for calculated and experimental spectra, respectively.

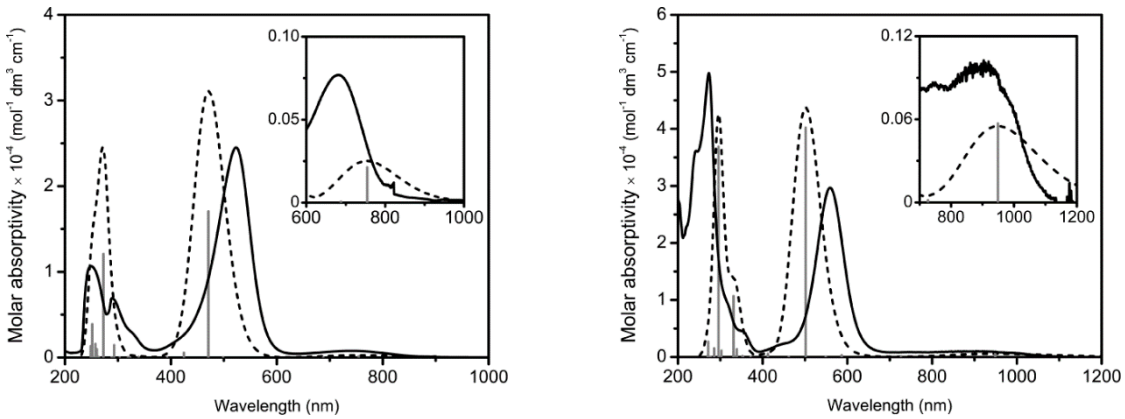

Figure S5: *TD-DFT calculated absorption spectra (dashed lines) with oscillator strengths (grey vertical lines) of CpCo(DAbnz) (left) and CpCo(DAnap) (right), compared with the experimental solution spectra (black lines). The full-width half-maximum (FWHM) values used for the calculated spectra were 3000* cm^{-1}.

Device Data

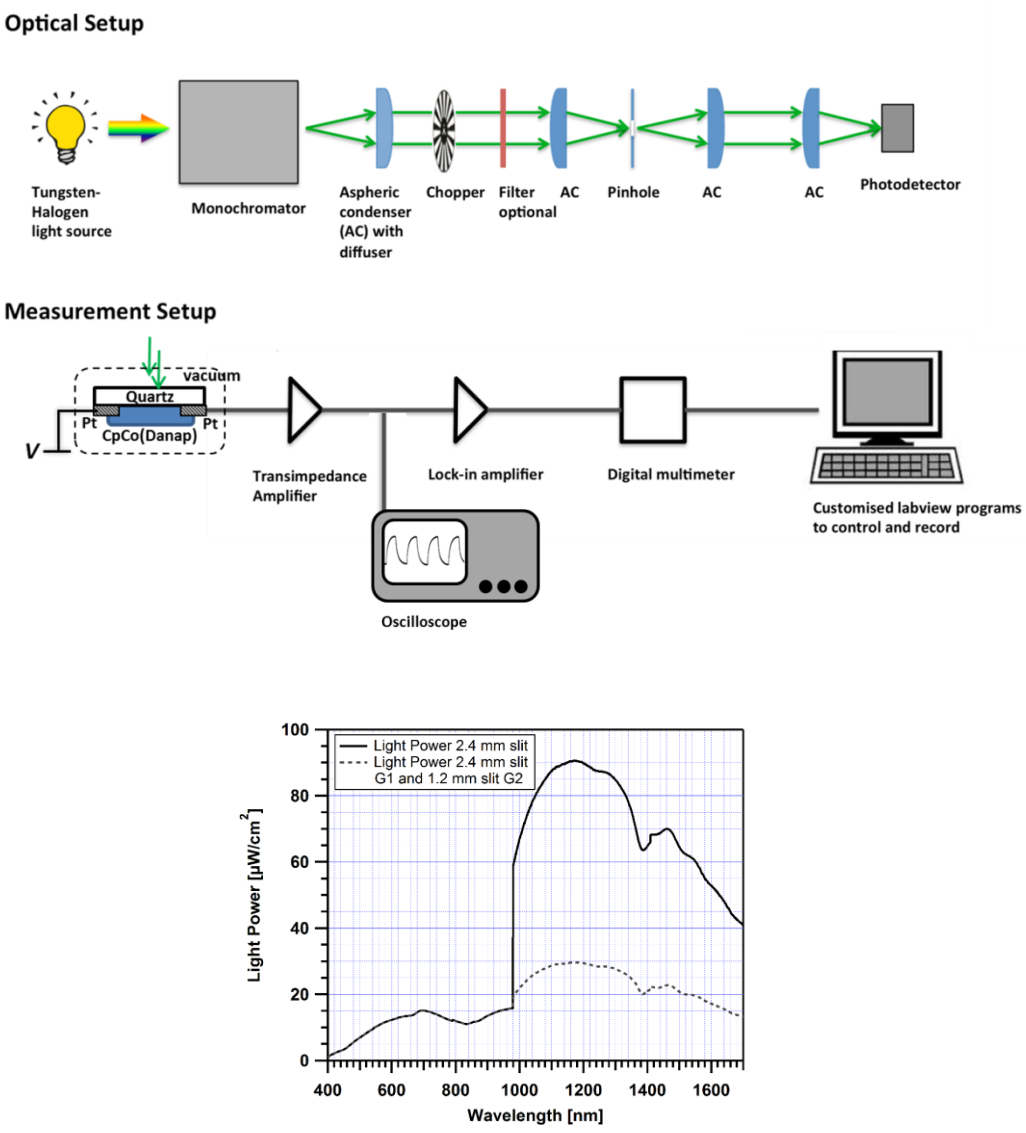

Figure S6*: (top) Optical setup for action photodetector measurements; (bottom) light power for action spectrum measurements.*

It should be noted that all devices measured showed a non-negligible decay in performance with time, decaying in a sublinear manner by ~50% over the first 1 hr, even under vacuum. While this could be corrected for by averaging the forward and reverse wavelength sweeps in the action spectra, it prohibited meaningful results in *I-V* sweep measurements, where the time dependence was more severe with increased bias, even in the absence of light.

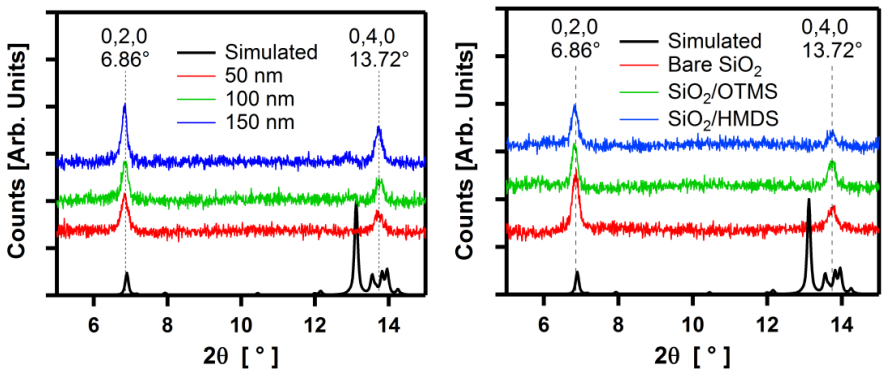

***Figure S7**: Thin film XRD of CpCo(DAnap) deposited (left) at a rate of 0.7 Ås^{-1} to different thicknesses on bare SiO_2 substrates, and (right) to 50 nm at a rate of 0.1 Ås^{-1} on surface modified SiO_2 substrates.*

***Table S9**: Figures of merit for transistors based on CpCo(DAnap)*

Deposition rate (As^{-1})	I_{on}/I_{off}	V_T (V)	μ_{lin} ($cm^2\ V^{-1}\ s^{-1}$)
0.2	10^5	-17	1×10^{-4}
0.7	10^5	-19	7×10^{-5}
1.5	10^5	-20	5×10^{-5}

*All of the electronic values were extracted from the transfer characteristics: I_{on}/I_{off} was calculated when the device is "on" at V_{GS} = -40 V and when the device is "off" at V_{GS} = 0 V; V_T was determined by extrapolating to the intercept a straight line fitted to the linear regime in the plot of I_{DS} against V_{GS}; μ_{lin} is calculated from the linear regime, where $\mu_{lin} = (dI_{DS}/dV_{GS})\cdot(L/C_iWV_{DS})$.

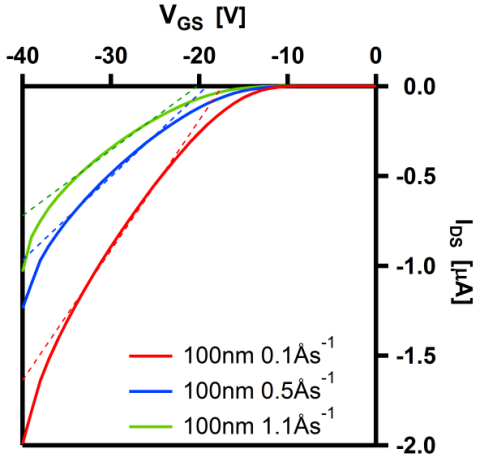

***Figure S8**: Transfer characteristics of CpCo(DAnap) deposited at rates of 0.2, 0.7 and 1.5 As^{-1} on HMDS treated substrates.*

Thin Film Data

CpCo(DAnap) deposited stably at each deposition rate, showing good agreement between theoretical thickness and mass deposited (as measured by the dissolved content over a defined substrate area). However, the real thickness, as measured by profilometry, showed a hyperbolic power dependence ($f(x) = A\cdot(x^p-1)$, where $p = 0.6$) to mass deposited. Figure S9 shows the discrepancy between real and modelled thickness, together with AFM images that reveal that in the early stages of growth, the material deposits as islands growing largely perpendicular to the substrate, before eventually coalescing as the film thickness increases. Such a deposition profile would account for the high failure rate of photodetectors formed from films <100 nm, as well as the discrepancy between real and theoretical thickness of the film, and would lead to significant pinholes in thin films, and/or poor substrate coverage at the semiconductor/SiO_2 interface, which is undesirable for device application.[5]

In an effort to improve the surface coverage at the interface, thin films were formed on octadecyltrimethoxysilane (OTMS) and HMDS treated SiO_2 substrates, and their structures analysed and compared to films on bare SiO_2. By thin film XRD, the crystallinity of films on ODTS was similar to that on bare SiO_2, while HMDS seemed to suppress the crystallinity of the CpCo(DAnap) (*c.f.* Figure S7). Figure S10(top) shows the AFM images of thin films deposited on the functionalized surfaces. Films fabricated on OTMS treated substrates showed an apparent increase in regularity of the particle morphology, compared to bare SiO_2, but with a greater propensity for growth perpendicular to the substrate. Comparison of the absorption spectra of the films grown on surface functionalized quartz substrates, shown in Figure S10(bottom), confirmed the similarity in growth for the SiO_2 and OTMS surfaces, with only a small change in their relative peak heights in the visible region, but a pronounced difference for the HMDS surface. Films on OTMS and bare SiO_2 showed little difference in the surface coverage at the substrate interface (65% by Bearing analysis as shown in Figure S11). In contrast, the surface coverage on HMDS was significantly increased (90%), with a pronounced reduction in particle size and regularity. Since the surface coverage on hydrophilic SiO_2 and hydrophobic OTMS was similar, one possible reason for the change in growth morphology on HMDS was the surface condition of the substrate. Despite depositing the HMDS by vapour methods, the surface quality of the bare substrate was shown to be distinctly less smooth (average roughness $R_z = 0.7$ nm) than for SiO_2 and OTMS ($R_z = 0.45$ and 0.5 nm respectively) (Figure S12 and Table S10), which might lead to better surface coverage through a greater number of seed points over the substrate. It seems, therefore, that the benefits of improved surface coverage outweigh those of a more crystalline film, since the average mobility of HMDS treated devices was about an order of magnitude improved from that of both ODTS and bare SiO_2 substrates. Furthermore, while a

shift in the threshold voltage to more negative values upon repeat testing was observed for all devices, this effect was less apparent for HMDS-treated substrates. Such a behaviour can be attributed to poor surface coverage on the dielectric, as shown by AFM analysis, which would result in weak electrostatic doping, and a distinctly non-linear doping of the channel, as evidenced by the non-linear drain current in the linear regime, and observed hysteresis.[5,6]

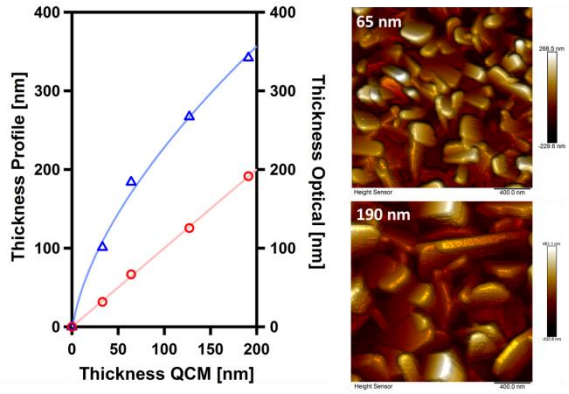

***Figure S9**: (left) Relationship between measured thickness (fit of $f(x) = A\cdot(x^p-1)$) and mass deposited (as measured by absorption spectroscopy of dissolved film) (linear fit) to target thickness from QCM for various thicknesses of CpCo(DAnap) deposited at a rate of 0.7 As^{-1}; (right) AFM images (2 x 2 μm) taken for different stages of growth for CpCo(DAnap) deposited at a rate of 0.7As^{-1}, at target thicknesses of 65 and 190 nm.*

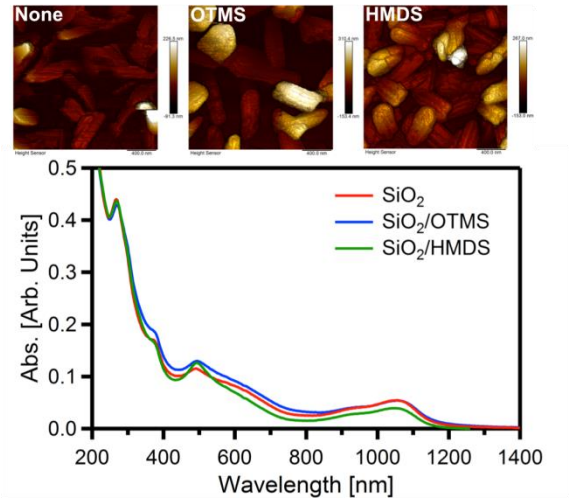

***Figure S10**: (top) AFM images (2 x 2 μm) of thin films of CpCo(DAnap) deposited on SiO_2, OTMS and HMDS substrates, and (bottom) UV/Vis/NIR spectra of the same films deposited on surface functionalized quartz substrates.*

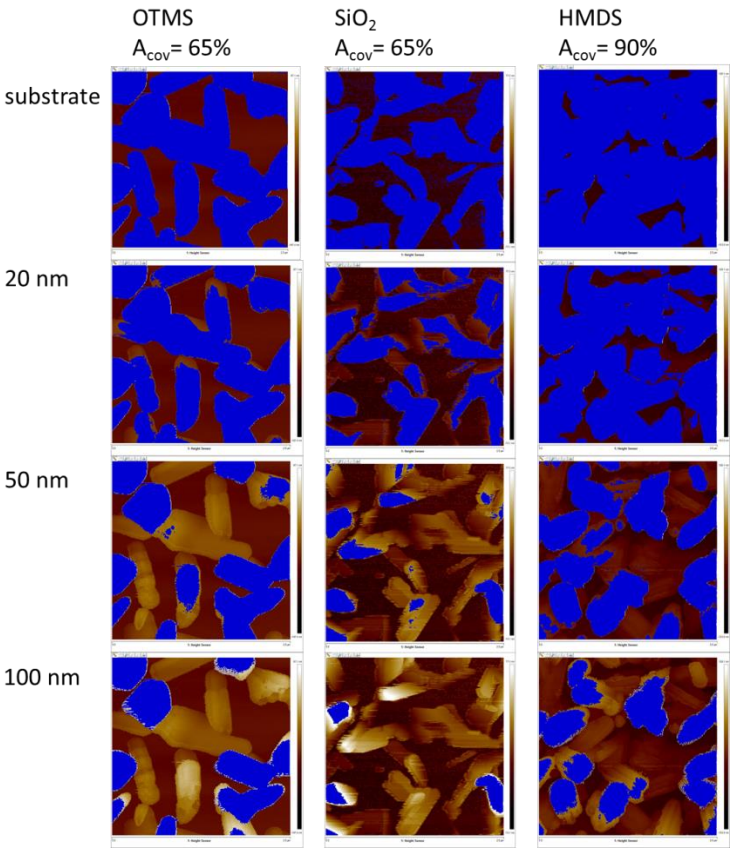

***Figure S11**: Bearing analysis of 20 nm thick films of CpCo(DAnap) deposited at 0.1 As^{-1} on OTMS and HMDS treated SiO_2, compared to bare SiO_2.*

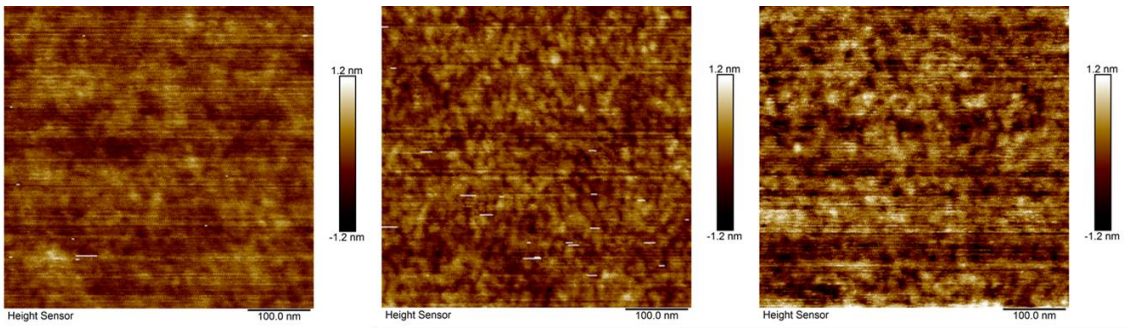

***Figure S12**: AFM images of bare SiO_2 substrate (left), compared to OTMS coated (middle) and HMDS coated (right) SiO_2.*

Table S10: *Roughness parameters, as estimated from AFM analysis for surface treated and bare SiO_2 substrates. Rmax is the difference between maximum valley depth and maximum peak height. Rz is the average from Rmax values. Ra is the arithmetic average roughness.*

	Rmax [nm]	**Rz [nm]**	**Ra [nm]**
SiO_2	0.9	0.45	0.1
OMTS	1.6	0.5	0.2
HMDS	2	0.7	0.2

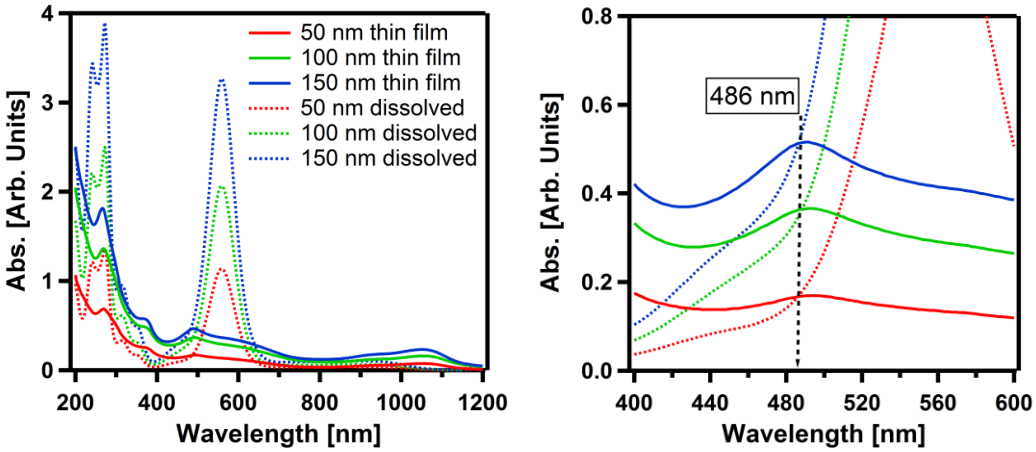

Figure S13*: (left) Absorption spectra of thin films of CpCo(DAnap) on quartz substrates, compared to dissolved films; (right) expansion of common intercept between thin film and solution data.*

References

1 R. B. King, *Inorganic Chemistry*, 1966, **5**, 82-87.

2 R. F. Heck, *Inorganic Chemistry*, 1968, **7**, 1513-1516.

3 M. Reinhardt, *Metal complexes containing non-innocent ligands for functional materials*, Doctoral thesis, University of Edinburgh, UK, 2012.

4 A. L. Rheingold, W. C. Fultz, T. B. Brill and S. J. Landon, *Journal of Chemical Crystallography*, 1983, **13**, 317-323.

5 D. Gupta, M. Katiyar and D. Gupta, *Organic Electronics*, 2009, **10**, 775-784.

6 P. B. Shea, J. Kanicki and N. Ono, *Journal of Applied Physics*, 2005, **98**, 014503.